

Origin of discrete electrical switching in chemically heterogeneous vanadium oxide crystals

B. Raju Naik¹, Yadu Chandran¹, Kakunuri Rohini¹, Divya Verma¹, Shriram Ramanathan², Viswanath Balakrishnan^{1*}

¹School of Mechanical and Materials Engineering, Indian Institute of Technology, Mandi, Himachal Pradesh-175075, India.

²Department of Electrical and Computer Engineering, Rutgers State University, New Jersey, Piscataway, NJ 08854.

*Corresponding author email: viswa@iitmandi.ac.in

Abstract:

Electrically driven insulator-metal transitions in prototypical quantum materials such as VO₂ offer a foundational platform for designing novel solid-state devices. Tuning the V: O stoichiometry offers a vast electronic phase space with non-trivial collective properties. Here, we report the discovery of discrete threshold switching voltages (V_{IMT}) with constant ΔV_{IMT} between cycles in vanadium oxide crystals. The observed threshold fields over 10000 cycles are $\sim 100X$ lower than that noted for stoichiometric VO₂ and show unique discrete behaviour with constant ΔV_{IMT} . We correlate the observed discrete memristor behaviour with the valence change mechanism and fluctuations in the chemical composition of spatially distributed VO₂-V_nO_{2n-1} complex oxide phases. Design of chemical heterogeneity in Mott insulators, therefore, offers an intriguing path to realizing low-energy neuromorphic devices.

Keywords: Chemical heterogeneity, metal-insulator transition, vanadium oxide, memristor, stochastic switching.

Insulator-metal transition (IMT) materials such as VO₂ show abrupt changes in electrical conductivity under electrical or thermal stimulus and are of interest as building blocks for artificial neurons¹⁻³. Intermediate metastable states might further be of interest for synaptic plasticity⁴⁻⁷. Most research on electrical switching characteristics has focused on phase pure

compounds of varying strain, dimensionality, W, Al, or oxygen vacancy-doped vanadium dioxide⁸⁻¹¹. Compositional heterogeneity within a single device channel to optimize the switching voltages represents an early research stage and could lead to reduced threshold switching energies compared to pristine single crystal bulk compounds. It is known that heterophase boundaries play a critical role in creating residual filaments that can help guide conductive filament nucleation¹²⁻¹⁶. Crystalline VO₂ is a potential candidate for engineering phase boundaries, mainly because the system can accommodate large vacancy concentrations and host numerous Magnéli-Wadsley phases at different V:O ratios¹⁷⁻²⁰. From a material's design perspective, understanding switching mechanisms and electrical properties in heterophase mixtures is essential in optimizing Mott devices. While non-stoichiometry might often be considered a detriment to device function, it is being increasingly examined as a feature in emerging devices, and our results provide a path for reduced switching energies and discrete switching that could be of interest in stochastic circuits.

This article demonstrates a threshold-switching device with discrete V_{IMT} voltages in chemically heterogeneous vanadium oxide single crystals and polycrystalline samples of in-plane and out-of-plane device geometries. Discrete switching at ultra-low voltages in non-stoichiometric vanadium oxide with spatial distribution of VO₂ and V_nO_{2n-1} heterophase is caused by electrically driven compositional fluctuations. The number of discrete switching points found in single crystalline samples is significantly higher when compared to the polycrystalline sample. Switching tests conducted over 10,000 I-V cycles show reduced discrete switching points, and eventually, the discrete V_{IMT} voltages are stabilized to a single point. The discrete stochastic switching mechanism was explained by population dynamics of electrochemical species and fluctuations in their valence states under applied electric field stress. This implies that during continuous electric bias switching cycles, the vanadium oxide

crystal experiences compositional changes dynamically. Microstructural design of heterogeneity in the V:O system is a promising direction to explore for threshold switching devices with stochastic threshold voltages that are discretized over a large number of cycles. The investigated aspects are also relevant for the fabrication of stoichiometric VO₂ thin film devices to enable stable threshold switching over a large number of cycles under optimal unipolar electric fields.

Results and Discussion

Figure 1a illustrates the graphical representation of two terminal device on a single crystal VO₂ fabricated with an approximate channel length of 40 μm and thickness of 600 nm (Figure S1a-b, Supporting Information). The vapor phase-grown vanadium oxide crystal exhibits distinct dark and bright patterns with random orientations. These contrasting regions are labelled as VO₂ (vanadium dioxide) and V_nO_{2n-1} (Magnéli phase vanadium oxide), which signifies the chemical heterogeneity within the crystal. This in-plane device structure has titanium/gold (Ti/Au) as contact electrodes. For electrical characterization, tungsten tips with a tip radius of ~ 7 μm were placed on the Ti/Au electrodes, and voltage was applied across the electrodes while the current passing through the crystal was limited by a set compliance value (I_{cc} = 10 mA). Figure 1b shows representative current versus voltage (I-V) characteristics in linear and semi-log plots (inset). The V_{IMT} (Insulator-Metal Transition) and V_{MIT} (Metal-Insulator Transition) voltages are defined as the specific voltages at which vanadium oxide exhibits a transition in its resistance states, transitioning from a high resistance insulating state to a low-resistance metallic state and, conversely, from metallic to insulating state. Interestingly, multiple current jumps are observed at discrete voltages (V_{IMT}), while no considerable variations are seen at V_{MIT}. It is known that oxygen deficiencies highly influence the structural stability and IMTs and in turn can reduce the threshold fields significantly. The single crystal device exhibits a large number of discrete IMT switching points (nearly ~9) within the first

100 I-V cycles, with a consistent voltage difference (ΔV_{IMT}) between cycles, which is an intriguing behaviour in VO₂. The marked numbers indicate the direction of the current flow in Figure 1b. For precise identification of discrete threshold voltages, all I-V plots are shown in linear scale, with a semi-log plot as inset for visualization. The scatter plot in Figure 1c illustrates the V_{IMT} voltages as a function of the number of cycles, revealing a ΔV_{IMT} of 0.74 V. In this study, it is observed that from the first initial 100 I-V repetitive cycles, the voltage needed for IMT is significantly smaller compared to stoichiometric VO₂. Also, the magnitude of resistance change in the insulator to metal is approximately 10^3 , which is one order less than stoichiometric VO₂. We performed material characterizations to investigate the origin of observed discreteness in voltages. Figure 1d shows an optical microscopy image of VO₂ single crystals with clear surface contrast in terms of dark and bright regions. We have used yellow and red arrows to illustrate the bright and dark regions within a VO₂ single crystal. FESEM image in backscattering mode (inset) confirms the presence of compositional variations in the VO₂ single crystals. Further, X-ray photoelectron spectroscopy (XPS) analysis of the elemental composition showed that the single crystal sample comprises 67.6 at. % of +4 oxidation state and 32.3 at. % of +5 oxidation state indicates the mixed phase composition, as shown in Figure 1(e). The X-ray diffraction (XRD) analysis (Figure 1f) shows that the crystals are chemically heterogeneous, as evidenced by a low-intensity impurity peak denoted by '@', which corresponds to Magnéli phase oxide (V₂O₃). Detailed structural investigations were carried out by Raman spectroscopy within bright and dark regions (Figure S2a-b, Supporting Information). It has been reported that the lower frequency peaks correspond to V-V vibrations, while the higher frequency peaks ($> 300 \text{ cm}^{-1}$) correspond to V-O vibrations. Since the VO₂ crystals formed using CVD show microdomains with different optical contrasts, we performed Raman spectroscopy in both bright and dark regions. It has been observed that the V-V vibrations at 193 and 225 cm^{-1} have reversed intensity ratios at neighboring bright and dark regions of the

same VO₂ crystals. Also, the Raman modes of the V-O bond have shifted to lower frequencies. The reversal of intensity ratio of V-V dimers is attributed to the lattice strain present within the sample, affecting the out-of-plane vibrations in the c_R due to the shortening of V-O bonds²¹. Similarly, the shift in V-V and V-O vibrations to lower frequencies also relates to the oxygen deficiency in the sample²². Thus, comparing the Raman modes of both bright and dark regions, it can be concluded that the bright region is oxygen deficient compared to the dark region.

In addition, the heterogeneity of the single crystal VO₂ was verified and confirmed using various techniques, including energy dispersive spectroscopy (EDS) (Figure S3a-b, Supporting Information), differential scanning calorimetry (DSC) heating and cooling curves (Figure S4a-c, Supporting Information), and *in situ* electrical and mechanical testing (Figure S5a-c, Supporting Information). All these analyses confirm that the as-grown crystal is not fully stoichiometric VO₂, instead, it is non-stoichiometric, with majority of volume fraction is dominated by stoichiometric VO₂. We conducted similar experiments on polycrystalline samples to verify this unique discrete behaviour. Figure 2a shows the schematic of the electrical measurements conducted in an out-of-plane geometry, with polycrystalline (PC) VO₂ sandwiched between a bottom platinum (Pt) electrode and top Ti/Au electrodes. The obtained I-V characteristics for a repetitive cyclic voltage test over 100 cycles display similar conspicuous discreteness in V_{IMT} voltages, as shown in Figure 2b. Thus, the device V_{IMT} voltages are highly unstable and bounce back and forth with multiple I-V cycles. Interestingly, the ΔV_{IMT} between cycles remains constant for the polycrystalline VO₂ device. The same is consistent with our observation on single crystal VO₂, mentioned earlier. The scatter plot shows a ΔV_{IMT} of 1.02 V over 10000 cycles (Figure 2c). Despite the differences in device geometries, the single and polycrystalline VO₂ devices exhibit the same unique discreteness in V_{IMT} with the same equal ΔV_{IMT} behaviour during I-V cycles. The PC-VO₂ crystals were further verified by microscopic and spectroscopic analysis. Figure 2d shows the SEM image and indicates the

microparticle nature of the PC-VO₂. Figure 2e shows the XPS analysis with multiple oxidation states +3, +4, and +5. The XRD analysis shown in Figure 2f confirms that VO₂ predominantly dominates the sample. Based on the electrical measurements, it is possible to claim that low-field switching and discrete switching over many cycles are dominated by ionic transport, supported by sweep polarity-dependent electrical I-V measurements. Figure 3a shows I-V characteristics during a positive voltage sweep with multiple IMT switching points. Figure 3b shows stabilized I-V characteristics within 900-1000 cycles, and the scatter plot in Figure 3c shows V_{IMT} distribution over 1000 cycles. Similarly, during the negative sweep, the multiple discrete points quickly get stabilized to a single V_{IMT}, and the V_{IMT} distribution over 1000 cycles shows an early stabilization (Figure 3d-f). This provides clear insights into the electroforming of conducting filament with the aid of charge transfer and also reveals the effect of polarity on stochastic threshold switching during voltage sweeps. This suggests that the crystal undergoes compositional fluctuations during the electrical switching cycles especially when the polarity is changed. Dark and bright pattern motion dynamics further verify these compositional changes on single crystal VO₂ under microscopy during heating-cooling cycles (Figure S6a-g, Supporting Information). These motion dynamics are observed near room temperature and differ from the typical contrast variations from insulator-metal transition near 68 °C in VO₂ crystals (Figure S7a-c, Supporting Information). In earlier works, a systematic reduction in threshold voltage has been demonstrated by introducing oxygen vacancies in VO₂ by controlled annealing²³. Oxygen vacancies have been extensively studied for their effect on electrical transport in VO₂. For instance, excess oxygen vacancies increase the carrier concentration and promote metallicity, suppressing abrupt phase transition in VO₂²⁴. Electrochemical creation and annihilation of oxygen vacancies at the nanoscale by applying an electric field through AFM tip on VO₂ is known to affect the transport properties²⁵. The approach of engineering the stoichiometry in VO₂ by introducing either oxygen vacancies or

excess oxygen has been explored for stabilizing rutile or triclinic phases^{18,26}. Inherent structural stochasticity with four variants of the M1 phase during insulator–metal transition in VO₂ has been observed via *in situ* electrical triggering in TEM. However, it is unclear how the structural stochasticity is directly related to the threshold voltages, especially when a greater number of discrete threshold voltages are observed beyond four structural variants²⁷. Further, the electric field triggered the formation of V₅O₉, conducting filament in VO₂, also reported to contribute to non-volatile switching at low threshold voltages²⁹. Such non-stoichiometric phases promote resistive switching at very low voltages despite large channel lengths. Earlier reports found that a stoichiometric VO₂ demanded significantly high threshold electric fields in the range of 10⁶ to 10⁷ V/m³⁰. Conversely, chemically heterogeneous VO₂ shows a remarkable reduction of electric fields compared to stoichiometric VO₂. The estimated threshold electric fields for switching the device vary between 4 x 10⁴ V/m to 21 x 10⁴ V/m within the investigated 10000 I-V cycles for VO₂ single crystals with a channel length of ~40 μm. Similarly, very low threshold electric fields, varying between 0.6 x 10⁴ V/m to 2.6 x 10⁴ V/m, are observed over 10000 repeated I-V cycles in heterogeneous polycrystalline VO₂ film with a thickness of 250 nm in the out-of-plane geometry. Note that the estimation of threshold electric fields is carried out with the in-plane channel length of ~40 μm, and in reality, the actual channel length might be much lower as the conducting oxygen deficient Magnéli phase is spatially distributed on the surface of VO₂ single crystals.

We correlate the mechanism of low V_{IMT} voltages that show discreteness with constant ΔV_{IMT} with dynamic fluctuation in composition and related shuttling of oxygen ion vacancies. Figure 4 shows a schematic of the mechanism for discrete threshold voltages during reversible I-V sweeps. Figure 4a and Figure 4b show a representative I-V hysteresis curve with six segments of operation, and crystalline VO₂ with dark and bright patterns, respectively. Segment I-III is for a positive voltage sweep and IA-IIIa for a negative voltage sweep. During part I, the

reduction process occurs with the creation of oxygen vacancies. As the voltage increases, a conducting filament by V_nO_{2n-1} starts forming by migration of oxygen vacancies across VO_2 , as shown in Figure 4c. The V_nO_{2n-1} (bright region) filament formation is due to small volume fractions of Magnéli phases between VO_2 (dark region) as shown in Figure 4b marked region. This filament formation increases current rapidly, and Joule heating becomes significant to drive the subsequent growth of conducting filament³¹. These filaments act like a guiding path and their formations are sensitive to these dynamic fluctuations in oxygen ion vacancy concentration. In segment II, the insulator-metal transition is triggered once the required threshold voltage is reached, leading to an abrupt increase in current. During segment III, oxidation occurs, and these filaments start rupturing by annihilation of oxygen vacancies by migration of oxygen ions, which results in an abrupt decrease in current (Figure 4d). The above processes are also valid in the negative voltage direction. Since the reduction process and filament formation require more supply of oxygen vacancies over repeated electric cycles, the filament formation path becomes random, generating several V_{IMT} . On the contrary, for rupturing, even a little annihilation of oxygen vacancies can break the conducting filament, leading to constant V_{MIT} without much deviations. During repeated electrical cycles, the conducting filament thickness increases, which results in a decrease in V_{IMT} , which is evident from the results of both single and polycrystalline VO_2 samples.

Nevertheless, the origin of discreteness in V_{IMT} with an equal voltage difference between each consecutive current-voltage characteristic of VO_2 needs further validation. It is possible to correlate the electrochemical redox reaction during the electrical triggering and changes in threshold voltages. We use the Nernst equation to understand the mechanism described below.

$$E = E^o - \frac{2.303 RT}{zF} \log (K) \text{-----}(1) \text{ }^{32}$$

Where E= Formal potential, E^o = standard potential, K= reaction quotient, z = number of charge transfer, F = Faraday's constant (96500 C mol⁻¹) R = gas constant (8.314 J mol⁻¹K⁻¹)

and T= temperature (298K). To make the above expression relevant for gas phase reactions, the reaction quotient has to be expressed in partial pressures of reaction species instead of their ionic concentrations. For all reactions involving the formation of the Magnéli phase (V_nO_{2n-1}) in VO_2 , the expression can be simplified as shown below.

$$E = E^o - \frac{2.303 RT}{zF} \left[\frac{1}{2} P(O_2) \right] \text{-----}(2)$$

Assuming the constant E^o value of 0.34V for all reactions involving reduction of V^{+4} to V^{+3} with fractional charge transfer, formation of V_2O_3 , V_3O_5 , V_4O_7 , V_5O_9 etc., values of E, free energy changes ($\Delta G = - nFE$) are calculated and shown in supplementary Table S1. It is possible to evolve several phases derived from a parent structure by crystallographic shear (c.s). Such systematic composition variations have been demonstrated in TiO_2 by incorporating c.s structures. For example, Magnéli phases of Ti_nO_{2n-1} wherein n is varied from 4 to 9, resulting in derived structures from TiO_2 , a rutile type with regular crystallographic shear on (121) planes³³. Moreover, it is known that slight changes in composition can be accommodated by varying only the orientation without any changes in the number of c.s planes. As mentioned earlier, the recent in situ TEM investigation on VO_2 also captured orientation changes within four possible variants during electrical triggering. When the VO_2 undergoes slight reduction, the oxygen deficiency may be accommodated by disordered c.s. planes. As the oxygen deficiency increases, they form parallel ordered groups, forming lamellae structures³³. Eventually they grow in size and form micro domain texture, making the crystal to diphasic heterogeneous system. In the present case, we have observed lamellae-like structures with parallel microdomains of various sizes that are seen in optical and electron microscope images. TEM bright field images and selected area diffraction patterns with superlattice reflections of such micro domain structures in VO_2 crystals are shown in Figure S8, Supporting information in consistent with earlier work on Ti_nO_{2n-1} .³⁴ The revealed lamellar and micro domain structures in TEM bright field images, Figure S8(a) and Figure S8(b) along with the superlattice

reflections in electron diffraction patterns provide clear evidence for oxygen deficient heterogeneous structure of vanadium oxide.

Interestingly such heterogeneity can be achieved in both oxygen deficient and oxygenated VO_2 with excess oxygen. The stoichiometry of crystal can be varied by altering the steps on each c.s planes, keeping the same number of c.s planes. During the reduction and oxidation, creation of excess cation and/or oxygen may flow up or flow down the c.s. planes respectively during voltage sweeps instead of limited only to thermal processing at high temperatures. Note that such minute compositional variations, introduced by annealing at high temperatures with controlled partial pressure of oxygen are known to induced discretized free energy changes in $\text{Ti}_n\text{O}_{2n-1}$ ³³. In the present case, theoretical calculation shows similar feature of discrete free energy changes against their compositions with different n values for $\text{V}_n\text{O}_{2n-1}$ as shown in Figure 4e. It is known that stability range of each of these Magnéli phases will be small in the order of few kJ/moles. Since the variations in the compositions are minimal, the step heights are also very similar, 0.65 kJ/mole when n varies from 9 to 11. At the same time, for lower values of n, the composition variations and the related step heights are large, evident from Figure 4e. The presented free energy change against the composition for varied ratios of O/V is calculated with the fractional charge transfer, while the mentioned number of cycles is roughly approximated to correlate with the experimental observation of cycle-dependent V_{IMT} . Variation in the composition and valence state during repeated cycling influences the value of E and results in discrete free energy changes for forming several non-stoichiometric phases. Because the memristive switching effect in the transition metal oxide memories is often associated with the electrochemical valence change mechanism under electrical triggering, the threshold voltage, V_T , and E are correlated³⁵. The electrochemical valence state fluctuations may occur during the repeated electrical switching in VO_2 in the solid state. Such dynamic electrochemical changes are already reported in the literature for functional oxide-based

memristors³⁶. The observed discreteness in the V_{IMT} voltages that are seemingly random in their occurrence over 10,000 repeated cycles could be explained by the variation in species undergoing valence change and the formation of several non-stoichiometric Magnéli phases during positive and negative voltage sweeps. In this scenario, the actual triggering voltage will be a random variable $R(V_T)$, which may change due to the valence state reaction's highly repeated threshold voltage, V_x and formal potential (E). Note that any slight variation in the population dynamics of electrochemical species and their valence states between the positive and negative voltage sweeps would affect the V_T as per the following expression with definite voltage difference (ΔV_{IMT}) across multiple switching events.

$$R(V_T) = V_x \pm n \Delta V_{\text{IMT}} \text{-----}(3)$$

Here, the n is an integer ($n = 1, 2, 3, 4$, etc) related to the compositional variations in Magnéli phase (V_nO_{2n-1}) that forms the conducting channel during the switching cycles. The population dynamics of V^{+4} species undergoing valence state are stochastic but result in switching at discrete threshold voltages dictated by the driving force for electroforming of Magnéli phase channels. Further the ΔV_{IMT} is related to the step heights in free energy change plot (Figure 4e). The discreteness in threshold voltages with constant ΔV_{IMT} arises due to the dynamic changes in composition of Magnéli phase wherein ‘ n ’ takes larger values above 5. In other words, the mechanism of electrical switching at threshold voltage is governed by insulator-metal transition in VO_2 ; the discrete variation in threshold voltages is arising due to local filament formations and its fluctuations in composition, induced by electrical cycling.

Conclusion

Vanadium oxide devices exhibit discrete switching behaviour driven by local fluctuations in composition. Cyclic bipolar switching stability test over 10000 cycles show discrete threshold voltages for several thousand cycles while early stabilization of discrete switching is observed during unipolar switching and confirm the valence change mechanism based memristor performance. The variation in compositional changes and associated free energy changes of

Magnéli phases at specific O/V ratios during voltage cycling guides the switching events with equal ΔV_{IMT} . The chemical heterogeneity and the observed fluctuations in fractional valence states resulted in the predictable distribution of discrete V_{IMT} voltages. The demonstrated aspects may provide a novel platform for the practical threshold switching memristor device applications by exploiting the discrete pattern in the switching processes synergistically involving valence change and phase transition.

Materials and Methods

The VO₂ single crystals were grown by CVD using V₂O₅ powder precursor at 900 °C in 8 sccm of Ar gas for 2 hrs. Before introducing the powder precursor in the quartz tube, it was cleaned with Ar purging for 1 hr at 100 sccm of flow rate. Powder precursor was kept inside a quartz boat and placed over a quartz boat on high-temperature brick. Quartz substrate was kept 5 mm away from the powder precursor, and the temperature of the furnace was ramped from 25 °C to 900 °C with a ramp rate of 20 °C /min. The entire growth was carried out in a low-pressure environment with a pressure of 4×10^{-4} mbar. For a polycrystalline-VO₂, 100 nm platinum (Pt) was deposited on quartz substrate by DC magnetron sputtering, and the same growth conditions of single crystalline VO₂ were used with quartz/Pt substrate.

Device fabrication

The two terminal planar device geometry on VO₂ crystals were fabricated with a commercially purchased shadow mask. The length between two electrodes is 40 μm, and a 50 nm Au was deposited as electrode material using DC magnetron sputtering. For an out-of-plane device with a VO₂ memristor, devices were fabricated with a planar device structure. Quartz/Pt/VO₂/Au were used as the substrate and electrode materials, respectively. The metal Au electrodes were deposited on VO₂ crystals using a shadow mask by DC magnetron sputtering.

Materials characterization

The single crystal surface morphology was characterized using a Nikon optical microscope, and thickness was measured with atomic force microscope (AFM) by Bruker. High-resolution images, EDS analysis, and backscattering images were recorded by field emission scanning electron microscopy (FESEM) by Nova Nano SEM-450. Raman vibrational modes were obtained with Raman spectroscopy by Horiba Jobin Yvon at 532 nm laser, crystallographic information using powder X-ray diffraction (XRD) by Rigaku, and elemental analysis using X-ray photoelectron spectroscopy (XPS) by ThermoScientific. The phase transition confirmation of VO₂ was done using differential scanning calorimetry (DSC) by NETZSCH Geratebau GmbH. The site-specific nanoindentation was performed by using Hysitron triboindenter 950I. The VO₂ crystals grown on a quartz substrate were attached to an iron stub and placed on the magnetic stage. A minimum of 10 indents were performed on each dark and bright region. The details of phase transition confirmation and Raman spectrum in polycrystalline VO₂ are provided in Figure S9a-d, Supporting Information. The thickness of films and crystals were measured by atomic force microscopy (AFM) by Bruker Dimension ICON PT. The single crystal structural characterization of VO₂ is analysed by high resolution transmission electron microscopy (HR-TEM) FEI-Tecnai G2 20 S-TWIN.

Device characterization

Electrical I-V measurements were carried out using Keysight- source measure unit B2902A model at room temperature. Resistance temperature measurements were carried out by connecting a heating stage to the probe station. For all measurements, Ti/Au were used as the electrodes.

Data availability

All the data are available within the article and in the supplementary information.

Author contributions

B. R. N. carried out the research, starting from the sample preparation, material and device characterization, and involved in the entire investigation and prepared the original manuscript. Y.C. performed nanoindentation, nano-ECR measurements. R. R. carried out CVD growth experiments. Divya Verma recorded optical images of thermally-induced phase transition in VO₂ crystals. V. S. R. participated in the discussion and provided critical comments on developing a mechanistic understanding of the work. V. B conceptualized and supervised the overall work and was involved in the original manuscript preparation. All authors have contributed to manuscript writing, reviewing, and editing.

Competing interests

The authors declare no competing interests.

Supporting Information

Supplementary information is provided.

Acknowledgements

This work was supported by the STARS program of the Ministry of Education- India (No. IITM/MHRD-STARS/VB/295). The authors would also like to thank the Advanced Materials Research Centre (AMRC) and centre for design and fabrication of electronic devices C4DFED for providing instrument facilities at IIT Mandi. VB also acknowledges Prof. N. Ravishankar, Indian Institute of Science (IISc), for the helpful discussion.

References

1. Zhang, X. *et al.* An Artificial Neuron Based on a Threshold Switching Memristor. *IEEE Electron Device Lett.* **39**, 308–311 (2018).
2. Yu, H., Islam, A. N. M. N., Mondal, S., Sengupta, A. & Ramanathan, S. Switching Dynamics in Vanadium Dioxide-Based Stochastic Thermal Neurons. *IEEE Trans. Electron Devices* **69**, 3135–3141 (2022).
3. Yi, W. *et al.* Biological plausibility and stochasticity in scalable VO₂ active memristor neurons. *Nat. Commun.* **9**, (2018).
4. Deng, S. *et al.* Selective area doping for Mott neuromorphic electronics. *Sci. Adv.* **9**, 1–10 (2023).
5. Wang, Y. *et al.* Optoelectronic Synaptic Devices for Neuromorphic Computing. *Adv. Intell. Syst.* **3**, 2000099 (2021).
6. Li, C. *et al.* Short-term synaptic plasticity in emerging devices for neuromorphic computing. *iScience* **26**, 106315 (2023).
7. Brinkman, B. A. W. *et al.* Metastable dynamics of neural circuits and networks. *Appl. Phys. Rev.* **9**, (2022).
8. Bohaichuk, S. M. *et al.* Localized Triggering of the Insulator-Metal Transition in VO₂ Using a Single Carbon Nanotube. *ACS Nano* **13**, 11070–11077 (2019).
9. Kim, M. W. *et al.* Substrate-mediated strain effect on the role of thermal heating and electric field on metal-insulator transition in vanadium dioxide nanobeams. *Sci. Rep.* **5**, 1–10 (2015).
10. Lu, Q. *et al.* Metal–insulator transition tuned by oxygen vacancy migration across TiO₂/VO₂ interface. *Sci. Rep.* **10**, 1–7 (2020).
11. Hu, B., Zhang, Y., Chen, W., Xu, C. & Wang, Z. L. Self-heating and external strain coupling induced phase transition of VO₂ nanobeam as single domain switch. *Adv. Mater.* **23**, 3536–3541 (2011).
12. Li, Y. *et al.* Anomalous resistive switching in memristors based on two-dimensional palladium diselenide using heterophase grain boundaries. *Nat. Electron.* **4**, 348–356 (2021).
13. Sangwan, V. K. *et al.* Multi-terminal memtransistors from polycrystalline monolayer molybdenum disulfide. *Nature* **554**, 500–504 (2018).
14. Wang, L. *et al.* Artificial Synapses Based on Multiterminal Memtransistors for Neuromorphic Application. *Adv. Funct. Mater.* **29**, (2019).
15. Lanza, M. *et al.* Grain boundaries as preferential sites for resistive switching in the HfO₂ resistive random access memory structures. *Appl. Phys. Lett.* **100**, (2012).
16. Pan, C. *et al.* Coexistence of Grain-Boundaries-Assisted Bipolar and Threshold Resistive Switching in Multilayer Hexagonal Boron Nitride. *Adv. Funct. Mater.* **27**, (2017).
17. Walls, B. *et al.* VO_x Phase Mixture of Reduced Single Crystalline V₂O₅: VO₂

- Resistive Switching. *Materials (Basel)*. **15**, 1–14 (2022).
18. Shi, R. *et al.* Phase management in single-crystalline vanadium dioxide beams. *Nat. Commun.* **12**, 1–9 (2021).
 19. Zhang, Z. *et al.* Evolution of Metallicity in Vanadium Dioxide by Creation of Oxygen Vacancies. *Phys. Rev. Appl.* **7**, 1–13 (2017).
 20. Brückner, W. *et al.* The range of homogeneity of VO₂ and the influence of the composition on the physical properties. II. The change of the physical properties in the range of homogeneity. *Phys. Status Solidi* **29**, 63–70 (1975).
 21. Evlyukhin, E. *et al.* Directly measuring the structural transition pathways of strain-engineered VO₂ thin films. *Nanoscale* **12**, 18857–18863 (2020).
 22. Parker, J. C. Raman scattering from VO₂ single crystals: A study of the effects of surface oxidation. *Phys. Rev. B* **42**, 3164–3166 (1990).
 23. Zhang, J. *et al.* Evolution of Structural and Electrical Properties of Oxygen-Deficient VO₂ under Low Temperature Heating Process. *ACS Appl. Mater. Interfaces* **9**, 27135–27141 (2017).
 24. Moatti, A., Sachan, R., Gupta, S. & Narayan, J. Vacancy-Driven Robust Metallicity of Structurally Pinned Monoclinic Epitaxial VO₂ Thin Films. *ACS Appl. Mater. Interfaces* **11**, 3547–3554 (2019).
 25. Sharma, Y. *et al.* Nanoscale Control of Oxygen Defects and Metal-Insulator Transition in Epitaxial Vanadium Dioxides. *ACS Nano* **12**, 7159–7166 (2018).
 26. Zhang, S., Kim, I. S. & Lauhon, L. J. Stoichiometry engineering of monoclinic to rutile phase transition in suspended single crystalline vanadium dioxide nanobeams. *Nano Lett.* **11**, 1443–1447 (2011).
 27. Cheng, S. *et al.* Inherent stochasticity during insulator-metal transition in VO₂. *Proc. Natl. Acad. Sci. U. S. A.* **118**, (2021).
 28. Jeong, J. *et al.* Suppression of metal-insulator transition in VO₂ by electric field-induced oxygen vacancy formation. *Science (80-.)*. **339**, 1402–1405 (2013).
 29. Cheng, S. *et al.* Operando characterization of conductive filaments during resistive switching in Mott VO₂. *Proc. Natl. Acad. Sci. U. S. A.* **118**, (2021).
 30. You Zhou, Xiaonan Chen, Changhyun Ko, Zheng Yang, C. M. and S. & Ramanathan. Voltage-triggered Ultra-fast Metal-insulator Transition in Vanadium Dioxide Switches. *IEEE Electron Device Lett.* **34**, 220–222 (2013).
 31. Valle, J. *et al.* Spatiotemporal characterization of the field-induced insulator-to-metal transition. *Science (80-.)*. **911**, 907–911 (2021).
 32. Ciobanu, M., Wilburn, J. P., Krim, M. L., Cliffler, D. E. & Electrochemistry, C. I. N. *Fundamentals of Electrochemistry*. (Elsevier, 2007). doi:10.1016/B978-0-444-51958-0.50002-1.
 33. R.R. Merritt, B.G. Hyde, L.A. Bursill, D. K. P. The thermodynamics of the titanium + oxygen system: an isothermal gravimetric study of the composition range Ti₃O₅ to TiO₂ at 1304 K. *Philos. Trans. R. Soc. London. Ser. A, Math. Phys. Sci.* **274**, 627–661 (1973).

34. Bursill, L. A. & Hyde, B. G. Crystallographic shear in the higher titanium oxides: Structure, texture, mechanisms and thermodynamics. *Prog. Solid State Chem.* **7**, 177–253 (1972).
35. Lim, E. W. & Ismail, R. Conduction mechanism of valence change resistive switching memory: A survey. *Electron.* **4**, 586–613 (2015).
36. Andreeva, N. V., Ryndin, E. A., Mazing, D. S., Vilkov, O. Y. & Luchinin, V. V. Organismic Memristive Structures With Variable Functionality for Neuroelectronics. *Front. Neurosci.* **16**, 1–9 (2022).

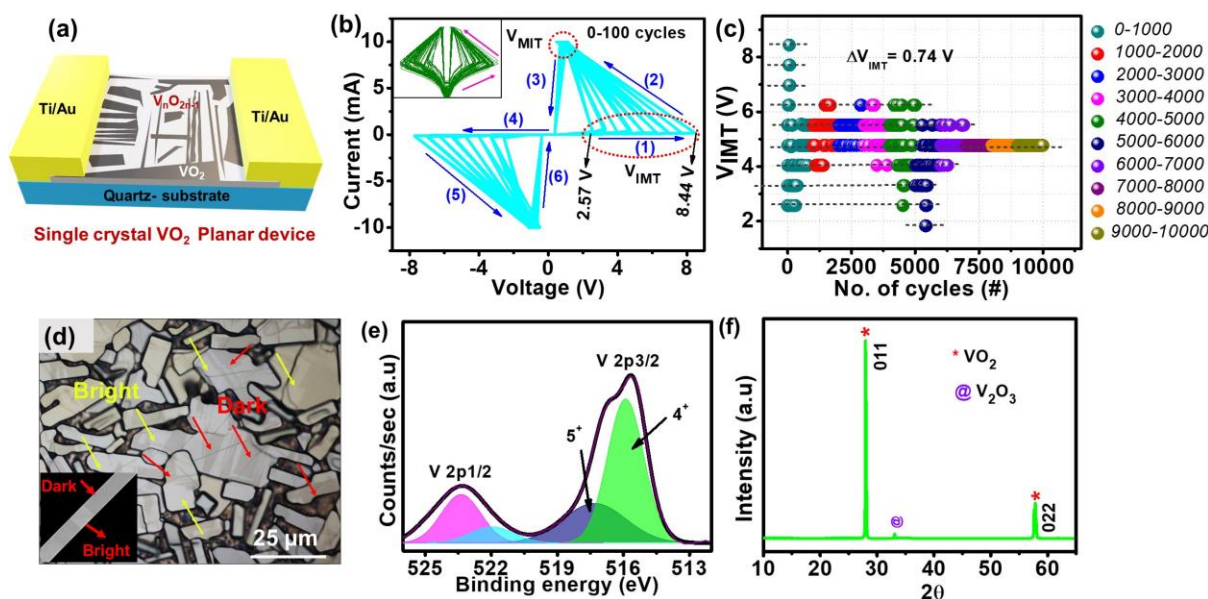


Figure 1. Depicts the scheme of the single crystal vanadium oxide device current-voltage measurements and their material characterizations. a) Schematic of chemically heterogeneous single crystal planar device, with an approximate channel length of $40\ \mu\text{m}$. b) I-V characteristics showing multiple transition points in the linear graph and inset shows semi-log plot. c) IMT scatter plot representing several I-V cycles vs. V_{IMT} , having ΔV_{IMT} of $0.74\ \text{V}$. d) Optical microscopy image of single crystals showing chemical heterogeneity (bright and dark patterns shown by yellow and red arrows) and inset shows the backscattering SEM image. e) V2p scan from XPS analysis representing multiple oxidation states (+4 and +5). f) XRD pattern confirming chemical heterogeneity with presence of Magnéli phase represented with symbol '@'.

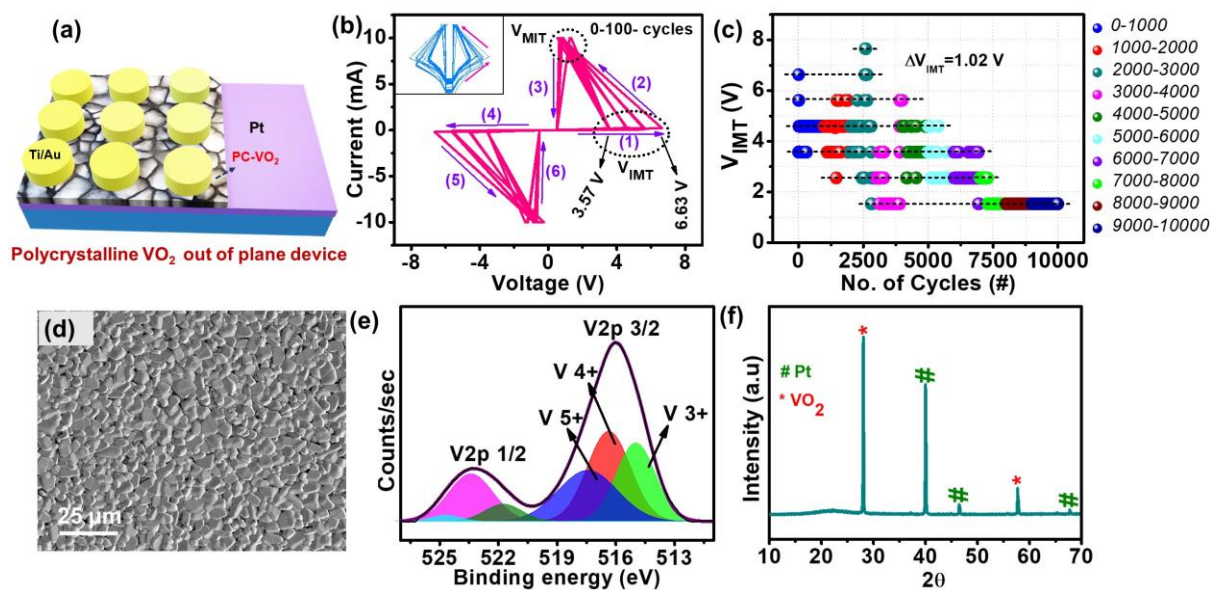


Figure 2. Depicts the vertical device current-voltage measurements of the poly crystalline vanadium oxide and their material characterizations. a) Schematic of polycrystalline out of plane device, with platinum and gold as top and bottom electrodes respectively. b) I-V characteristics showing multiple transition points in the linear graph and inset shows semi-log plot. c) IMT scatter plot representing several I-V cycles vs. V_{IMT} , ΔV_{IMT} of 1.02 V. d) SEM image of polycrystalline vanadium oxide showing grain like structures. e) V2p scan from XPS analysis representing multiple oxidation states (+3, +4 and +5). f) XRD pattern confirming the VO_2 .

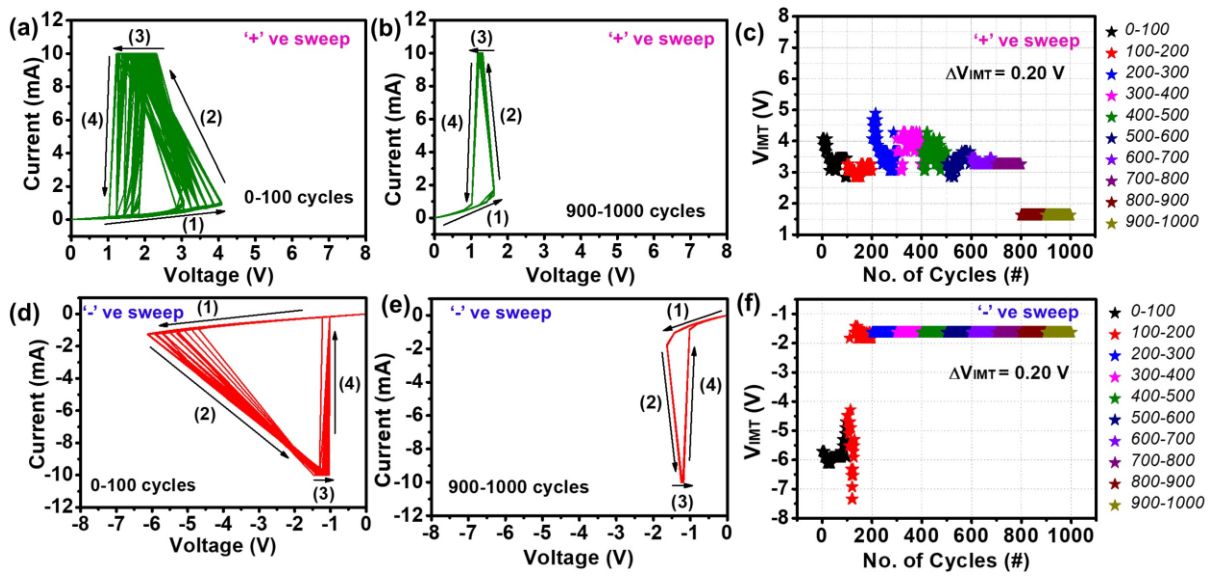


Figure 3. Sweep bias polarity dependent electrical transport measurements of single crystal vanadium oxide sample. a) Discrete IMT switching over initial 0-100 I-V cycles during positive sweep. b) Switching between 900-1000 cycles. c) Distribution of V_{IMT} voltages vs number of cycles with ΔV_{IMT} of 0.20 V. d) Discrete switching in negative sweep for initial 0-100 cycles. e) Switching between 900-1000 cycles. f) Distribution of V_{IMT} voltages vs number of cycles with ΔV_{IMT} of 0.20 V.

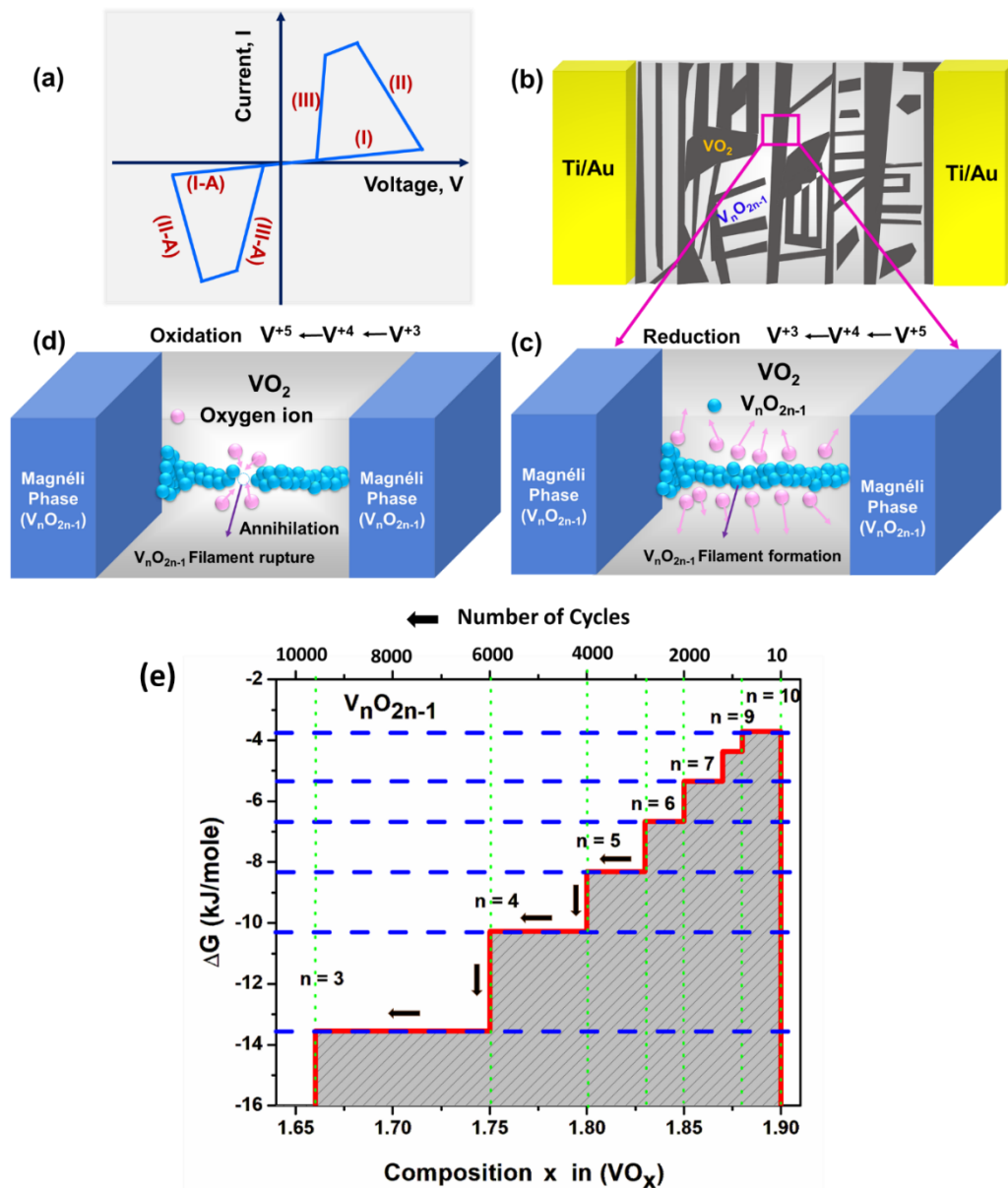


Figure 4. Schematic illustration of the conduction mechanism of chemically heterogeneous vanadium oxide with the help of oxygen vacancies and ionic movement. a) Schematic of I-V hysteresis. b) Schematic representation of chemically heterogeneous vanadium oxide device with bright and dark patterns. c) I and I-A represent the vacancy-induced filament formation across Magnéli phases, and II and II-A represent the phase change of VO₂. d) III and III-A represent the filament rupturing due to vacancy annihilation. (e) Discrete free energy changes against compositional evolution are observed during electrical switching cycles. The discrete free energy changes with respect to the composition of complex oxides are calculated for redox reactions involving fractional charge transfers, while the mentioned number of cycles is approximate based on experimental observations.